



Power Electronic Systems
Laboratory

© 2021 IEEE

Proceedings of the 36th Applied Power Electronics Conference and Exposition (APEC 2021), June 14-17, 2021

Single-Phase Full-Power Operable Three-Phase Buck-Boost Y-Rectifier Concepts

D. Menzi,
J. W. Kolar,
J. Everts

Personal use of this material is permitted. Permission from IEEE must be obtained for all other uses, in any current or future media, including reprinting/republishing this material for advertising or promotional purposes, creating new collective works, for resale or redistribution to servers or lists, or reuse of any copyrighted component of this work in other works.



Eidgenössische Technische Hochschule Zürich
Swiss Federal Institute of Technology Zurich

Single-Phase Full-Power Operable Three-Phase Buck-Boost Y-Rectifier Concepts

D. Menzi, J.W. Kolar
 Power Electronic Systems Laboratory (PES)
 ETH Zurich
 Zurich, Switzerland
 menzi@lem.ee.ethz.ch

J. Everts
 Prodrive Technologies B.V.
 Eindhoven, Netherlands

Abstract—Future electric vehicle chargers should feature full nominal output power in single-phase (1- Φ) and three-phase (3- Φ) operation, such that they can be employed in the USA as well as in Europe. Further, the converter system should have buck-boost capability to cover a wide DC output voltage range in order to provide compatibility with various nominal battery voltage levels. The phase-modular Y-Rectifier consists of three buck-boost converter modules, features unity power factor operation and allows for an ultra-compact and highly efficient converter realization, where so far only 3- Φ operation was investigated in literature. In this paper, circuit extensions adapting the Y-Rectifier for both 1- Φ and 3- Φ operation are analyzed and comparatively evaluated, where also a new six-module Y-Rectifier (6M-YR) topology is proposed. The required modulation and control techniques of the 6M-YR are presented for 1- Φ and 3- Φ operation. The discussed topologies are then compared by means of a component current conduction stress and a power stage performance analysis for a 6.6 kW, 3- Φ 400 V (Europe) / 1- Φ 240 V (USA) AC, 200 V to 750 V DC application. Further, EMI filter design guidelines for the 6M-YR are presented. The results indicate the feasibility of a highly compact CISPR 11 Class B compliant 6M-YR with a power density of 10 kW/dm³ (164 W/in³) and a nominal efficiency of 98.1% in 3- Φ and 97.6% in 1- Φ operation.

Index Terms—EV charger, AC/DC converter, buck-boost Y-rectifier, six-module, single-phase, three-phase

I. INTRODUCTION

In order to support further proliferation of Electric Vehicles (EVs), future on-board battery chargers should allow for nominal power operation when connected to the European three-phase (3- Φ) grid (400 V_{rms} line-to-line voltage [1]), as well as for operation in a US American split single-phase (1- Φ) grid ($2 \cdot 120$ V_{rms} = 240 V_{rms} line-to-line voltage [2]). According to Refs. [3] [4] a typical 3- Φ rectifier system (cf. **Fig. 1a**) can operate in a 1- Φ grid as depicted in **Fig. 1b** by attaching one phase terminal to line g and another phase terminal to neutral N and leaving the third phase terminal without connection. Using this arrangement, only approximately 1/3 of the nominal output power can be provided, or a massive overdimensioning of the employed components is required to allow full rated power 1- Φ operation.

Charging systems are required to cover a wide DC output voltage range of typically 200 V to 750 V [5] in order to allow compatibility with various EV battery nominal voltages, and accordingly, buck-boost capability is required. As Power

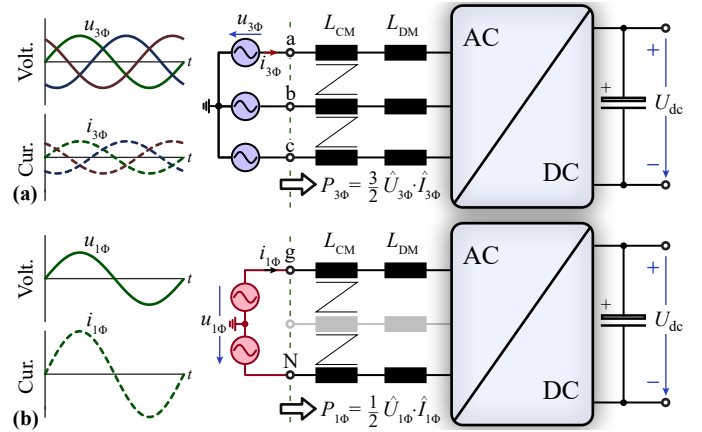


Fig. 1: 3- Φ rectifier running in (a) 3- Φ operation (Europe) where the three converter input terminals are attached to the grid phases a, b, c and (b) 1- Φ operation (USA), where only two converter terminals are connected to grid line g and neutral N , while the third terminal is left without connection.

Factor Correction (PFC) rectifier systems are typically limited to either buck or boost operation [6], an additional DC/DC converter stage has to be provided to comply with a wide DC output voltage range as e.g. specified in [5]. In contrast, consisting of three buck-boost converter phase modules, the phase-modular 3- Φ Three-Module Y-Rectifier (3M-YR) [7] [8] features DC output voltages both above or below the grid voltage amplitude without the need for an additional DC/DC converter stage. In each phase module either the buck-stage or the boost-stage is operated with Pulse Width Modulation (PWM) depending on the instantaneous input-output voltage ratio. As both stages are active in a mutually exclusive way and the inductor is shared by both stages, effectively a single-stage energy conversion is achieved and an ultra-compact and highly efficient converter realization is facilitated. However, the 3M-YR so far was only investigated for 3- Φ operation.

In this paper, we analyze the 1- Φ operation of Y-Rectifier concepts, first considering a circuit extension of the 3M-YR [7] in **Sec. II**. Subsequently, in **Sec. III** we propose a new Six-Module Y-Rectifier (6M-YR) topology enabling 1- Φ operation without the need for additional circuitry and/or modified Electromagnetic Interference (EMI) filter structure and with

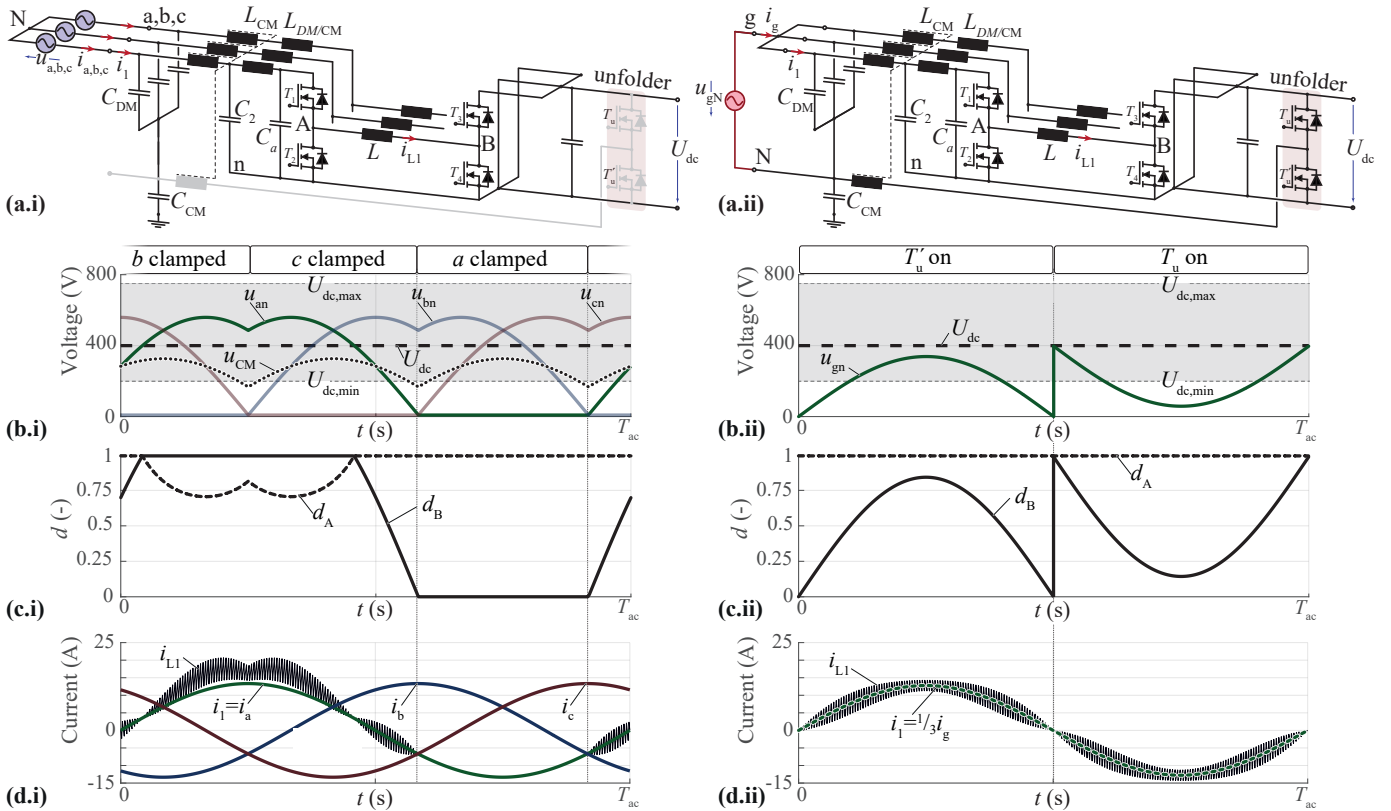


Fig. 2: (a) Circuit diagram of the proposed 3M-YR-U with an unfold bridge-leg conceptually based on [9]: (a.i) 3- Φ operation (with the neutral terminal N not connected, and the unfold bridge-leg disabled) and (a.ii) 1- Φ operation (with three paralleled phase modules connected to the grid phase terminal g and active unfold bridge-leg attached to N). Corresponding main converter waveforms in 3- Φ (400 V_{rms} line-to-line, 230 V_{rms} phase voltage) and 1- Φ operation (240 V_{rms} line-to-neutral voltage) for $U_{dc} = 400$ V and output power $P = 6.6$ kW: (b) characteristic voltages, (c) buck stage d_A and boost stage d_B duty ratios of the module #1, and (d) phase currents.

reduced component stresses. The considered topologies are compared in terms of conduction stresses and the power-stage performance of virtual prototypes in both 1- Φ and 3- Φ operation in Sec. IV. Then, in Sec. V the EMI filter design process for the 6M-YR is discussed and finally, in Sec. VI a conclusion is presented.

II. Y-RECTIFIER WITH ADDITIONAL UNFOLDER BRIDGE-LEG (3M-YR-U)

Recent literature [9] suggests extending a 3- Φ PFC converter with an unfold bridge-leg, which connects to neutral N in 1- Φ operation. Furthermore, the 3- Φ Common Mode (CM) EMI filter inductor is extended with a fourth winding placed in the neutral connection in order to prevent saturation for 1- Φ operation. This concept is also applicable to the 3M-YR, and the resulting main power circuit including three buck-boost modules referenced to the negative DC-link rail n , an unfold bridge-leg and the modified EMI filter structure – further denoted as 3M-YR-U – is outlined in Fig. 2a.

In 3- Φ operation (cf. Fig. 2a.i) the neutral terminal N is not connected, while the phase modules are attached to the respective grid terminals a, b, c . Modulation is performed according to [7] and Fig. 2b.i-d.i presents the relevant converter waveforms for operation with $U_{3\Phi} = 230$ V_{rms}, $U_{dc} = 400$ V and output power $P = 6.6$ kW: The input voltages

u_{an}, u_{bn}, u_{cn} in Fig. 2b.i are strictly positive and contain a time varying offset voltage $u_{CM} = (u_{an} + u_{bn} + u_{cn})/3$ allowing discontinuous PWM [10]. The module with the lowest input voltage is clamped to the negative DC-link rail (i.e. T_1 and T_4 permanently on) during 1/3 of the fundamental period, allowing for PFC operation with a substantial switching loss reduction of at least 1/3 compared to standard sinusoidal PWM. For the considered operating point, input voltages both above and below the DC output voltage result and Fig. 2c.i presents the buck stage d_A and boost stage d_B duty ratios of the converter module #1. Each module conducts the respective line current i_a, i_b, i_c (i.e. for module #1 the input current is given by $i_1 = i_a$) and Fig. 2d.i further shows the inductor current i_{L1} of module #1, which is elevated compared to i_1 in buck operation [7].

Then, for 1- Φ operation, the converter phase modules are paralleled and connected to the grid line terminal g , and the unfold bridge-leg output is connected to the neutral terminal N as highlighted in Fig. 2a.ii. The converter waveforms are presented in Fig. 2b.ii-d.ii: The unfold bridge-leg operates on a fundamental frequency level and connects the neutral terminal N with the negative DC-link rail n (T'_u on) for grid voltages $u_{gN} \geq 0$, and with the positive DC-link rail (T_u on) for $u_{gN} < 0$. In contrast to 3- Φ operation, the common mode voltage u_{CM} is defined by the unfold operation and all three

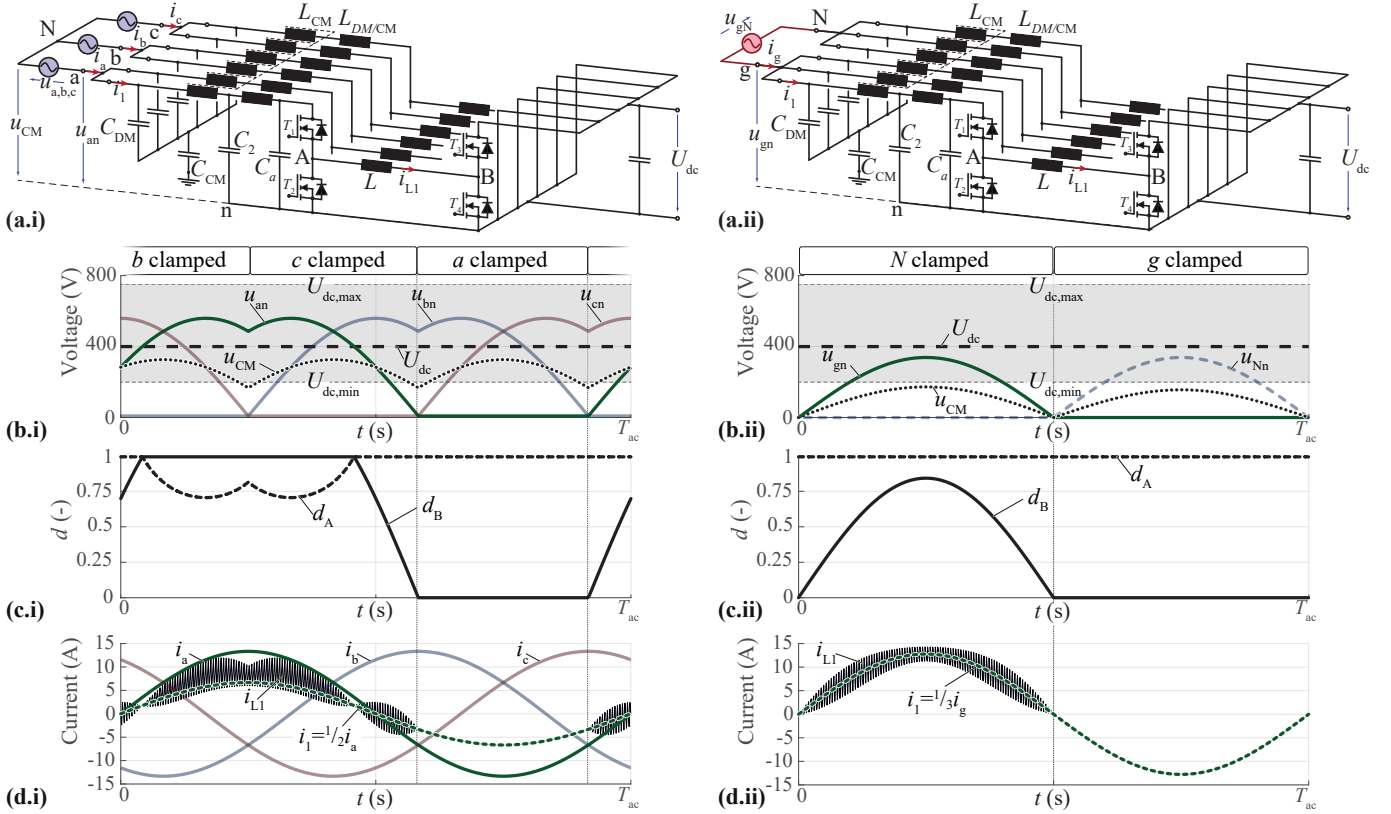


Fig. 3: (a) Circuit diagram of the proposed 6M-YR configuration: (a.i) 3- Φ operation (with 3x2 paralleled modules) and (a.ii) 1- Φ operation (with 2x3 paralleled modules connected to the line g and neutral N grid terminal). Corresponding main converter waveforms in 3- Φ (400 V_{rms} line-to-line, 230 V_{rms} phase voltage) and 1- Φ operation (240 V_{rms} line-to-neutral voltage) for $U_{dc} = 400$ V and output power $P = 6.6$ kW: (b) characteristic voltages, (c) buck stage d_A and boost stage d_B duty ratios of module #1, and (d) phase currents.

modules operate permanently with PWM. The grid current i_g is equally shared between the modules (i.e. $i_1 = i_g/3$), such that 1- Φ operation with full nominal power is enabled without component overdimensioning. However, using this approach an extension of the basic 3M-YR structure with dedicated additional circuitry (unfolder) is required and modularity is partially lost. Further, given the strictly positive converter input voltages, the 3M-YR-U is limited to DC output voltages larger than the grid peak AC voltage. This becomes obvious when considering the input voltage in Fig. 2b.ii which is limited to values $u_{gn} \in [0, U_{dc}]$ within the second half-period. Hence, in contrast to the 3M-YR, the 3M-YR-U in 1- Φ operation only offers boost functionality: When considering a current controllability margin the DC voltage range is limited in practice to $U_{dc,min} \approx 400$ V for a grid voltage $U_{1\Phi} = 240$ V_{rms}.

III. SIX-MODULE Y-RECTIFIER (6M-YR)

In order to comply with the above mentioned EV charger specifications while maintaining full modularity and/or for avoiding additional circuitry, we propose another modification of the 3M-YR topology – the Six-Module Y-Rectifier (6M-YR) – where only the arrangement of the phase modules is adapted for 3- Φ (3x2 parallel modules) and 1- Φ operation (2x3 parallel modules) using e.g. relays or simple mechanical contacts. The resulting main power circuit where six buck-boost phase-modules are referenced to the negative DC-link rail n is

outlined in Fig. 3a, where the EMI filter structure includes a six-winding CM choke, making the CM filter effective both in 1- Φ and 3- Φ operation. The respective terminal voltage, duty cycle and current waveforms are depicted in Fig. 3b-d.

In 3- Φ operation (cf. Fig. 3a.i-d.i), $k_{3\Phi} = 2$ converter modules are connected in parallel to each grid phase terminal, hence equally sharing the grid phase current and resulting in $i_1 = i_a/2$ for a single module. Again, discontinuous PWM can be facilitated, where the two modules of the phase with the lowest input voltage are clamped during 1/3 of the fundamental period.

The 6M-YR in 1- Φ operation is depicted in Fig. 3a.ii, where the converter is reconfigured such that $k_{1\Phi} = 3$ converter modules are connected in parallel to each grid phase terminal and the elevated 1- Φ grid current is advantageously shared among them and $i_1 = i_g/3$. As now, different to Fig. 1b, the modules of all phases are active, the converter reconfiguration allows to reduce the filter component over-dimensioning for nominal output power 1- Φ operation. Note that (as for the 3M-YR) a terminal voltage offset with respect to the negative DC-link rail of $u_{CM} = \frac{1}{2}(u_{gn} + u_{Nn})$ cancels out and states a degree of freedom for the 1- Φ operation allowing to redistribute conduction and switching stresses among the power semiconductors of the phase modules. Advantageously, u_{CM} can be set as shown in Fig. 3b.ii such that only one out

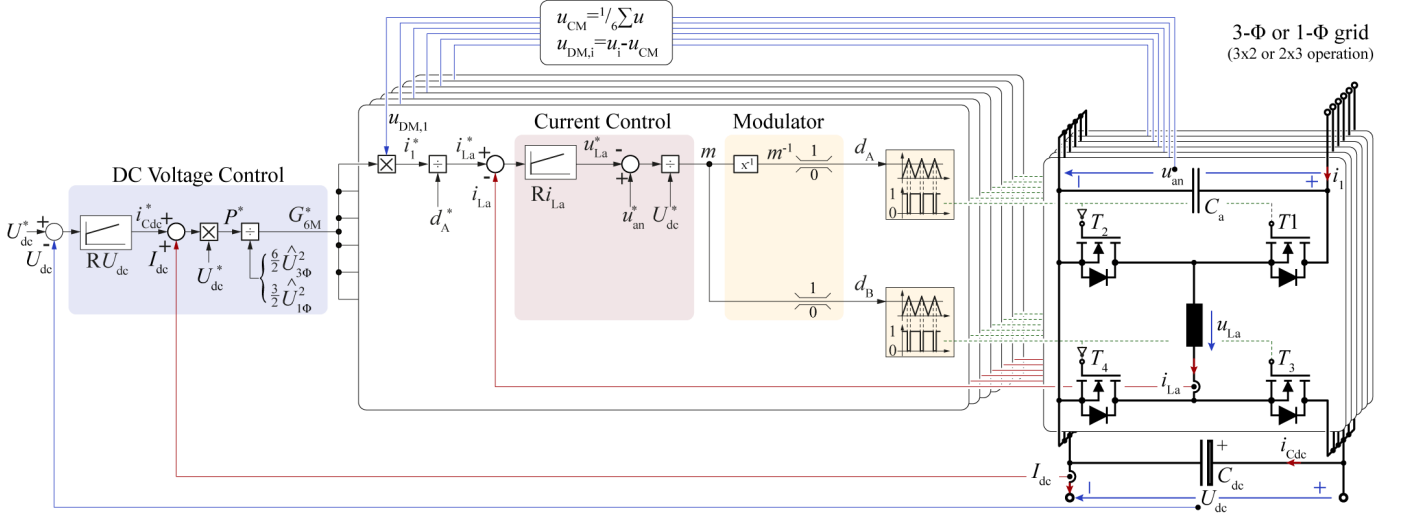


Fig. 4: 6M-YR cascaded DC output voltage control scheme for 3- Φ and 1- Φ PFC operation including the relevant control and measurement signals.

of the two module groups is PWM operated at any point in time (i.e. alternating every grid half period), hence reducing semiconductor switching losses. Note that the 1- Φ input capacitor voltages u_{gn} and u_{Nn} can also be formed for $U_{dc} < \hat{U}_{1\Phi}$, i.e. the 6M-YR provides full buck-boost functionality in 1- Φ operation.

Fig. 4, presents the phase-modular representation of the 6M-YR (only the circuit structure of module #1 is shown in detail), as well as the control diagram realizing the discussed modulation strategy in both 3- Φ and 1- Φ operation. The control structure comprises two cascaded control loops, and the DC voltage regulator sets an input power reference P^* based on the output voltage control error. Depending on the operation mode, a module conductance reference is calculated:

$$G_{6M}^* = \begin{cases} \frac{P^*}{6/2\hat{U}_{3\Phi}^2} & 3\text{-}\Phi \text{ operation} \\ \frac{P^*}{3/2\hat{U}_{1\Phi}^2} & 1\text{-}\Phi \text{ operation} \end{cases} \quad (1)$$

The subsequent module control is identical for each module and hence only explained once for module #1. There, a sinusoidal module input current reference i_1^* is calculated by multiplying G_{6M}^* with the measured differential mode component of the module input capacitor voltage $u_{DM,1}$. Aiming at a simple and low-realization effort control strategy, the input current reference can be directly translated into an inductor current reference $i_{L,1}^* \geq i_1^*$ by division with the reference buck stage duty cycle d_A^* , i.e. by neglecting the current of the input capacitor C_a . The inductor current controller then outputs the modulation index m which can be translated by the modulator block [7] into duty cycles d_A and d_B assuring mutually exclusive operation of the buck and boost stage.

IV. PERFORMANCE COMPARISON

Tab. I recapitulates the number of paralleled modules in 3- Φ ($k_{3\Phi}$) and in 1- Φ operation ($k_{1\Phi}$) of the considered topologies. In the following, the performance of the 3M-YR (cf. Fig. 1), the 3M-YR-U (cf. Fig. 2a) and the 6M-YR (cf. Fig. 3a) in 3- Φ and

TABLE I: MODULE CONFIGURATION

	3M-YR	3M-YR-U	6M-YR
$k_{3\Phi}$	1	1	2
$k_{1\Phi}$	1	3	3
$k_{3\Phi}/k_{1\Phi}$	1	1/3	2/3

1- Φ operation is assessed by means of a current conduction stress analysis in Sec. IV-A and a virtual prototype power-stage efficiency and loss comparison in Sec. IV-B.

Fig. 5a depicts the considered DC output voltage and current range, where the maximum output power of 12.4 kW is provided for $U_{dc} = 750$ V (a DC current limit of 16.5 A applies, and for $U_{dc} < 200$ V the output current is further reduced). This corresponds to a 6.6 kW system according to [5] where nominal power is provided from 400 V to 750 V. Fig. 5b recapitulates the input capacitor voltage waveforms in 3- Φ and 1- Φ operation (note that the 3M-YR-U is limited to boost 1- Φ operation, i.e. can only operate for DC output voltages $U_{dc} > \sqrt{2} \cdot 240$ V_{rms}).

The considered design specifications and the main components of the power modules are listed in Tab. II. All designs employ a switching frequency of 100 kHz and the selected module inductance value for the 3M-YR and the 3M-YR-U is $L = 85$ μ H. Increasing the inductor value by a factor of two (i.e. $L = 170$ μ H), the same ratio of inductor maximum high-frequency peak current and fundamental-frequency current can be maintained in 3- Φ operation for the 6M-YR, hence allowing a fair comparison. Accordingly, an input capacitance value $C_a = 3.5$ μ F is selected for the 3M-YR and the 3M-YR-U, and $C_a = 1.7$ μ F for the 6M-YR, such that the 6M-YR design represents a scaled version of the 3M-YR with modules rated for half the nominal power. Since the resulting conduction stresses only depend on the component values, the practical converter component realization is discussed in detail in Sec. IV-B.

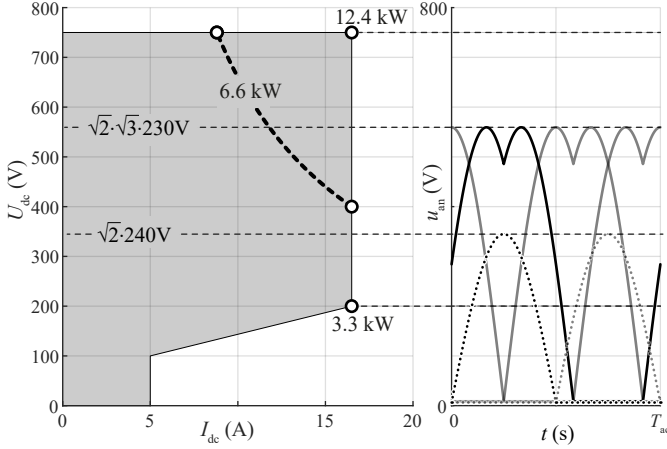


Fig. 5: (a) Considered DC output voltage and current range corresponding to a 6.6 kW system according [5] where nominal power is provided from 400 V to 750 V. Up to 12.4 kW output power can be provided for $U_{dc} = 750$ V (a DC current limit of 16.5 A applies) and for $U_{dc} < 200$ V the output current is further reduced. (b) Input capacitor voltages for 3- Φ and 1- Φ operation where the maximum input voltage represents the lower limit for boost operation.

A. Current Conduction Stress Comparison

For all considered topologies the module input current I_1 represents the predominant loss driver in the inductive components of the EMI filter (i.e. L_{CM} , $L_{DM/CM}$ in **Fig. 2a** and **Fig. 3a**) and is defined by

$$I_1 = \begin{cases} \frac{I_{3\Phi}}{k_{3\Phi}} = \frac{P}{k_{3\Phi} 3U_{3\Phi}} & 3\text{-}\Phi \text{ operation} \\ \frac{I_{1\Phi}}{k_{1\Phi}} = \frac{P}{k_{1\Phi} U_{1\Phi}} & 1\text{-}\Phi \text{ operation.} \end{cases} \quad (2)$$

For a given power level P and $U_{1\Phi} \approx U_{3\Phi}$, phase currents $I_{1\Phi} \approx 3 \cdot I_{3\Phi}$ result and hence the ratio $k_{3\Phi}/k_{1\Phi}$ (cf. **Tab. I**) is a key figure for the conduction stress increase in 1- Φ operation.

The main power component RMS current stresses of the considered topologies in 3- Φ and 1- Φ configuration for a grid line-to-neutral voltage of $U_{3\Phi} = 230 V_{rms}$ (corresponding to 400 V_{rms} 3- Φ line-to-line voltage) and $U_{1\Phi} = 240 V_{rms}$, respectively, a constant output power of 6.6 kW, and for a DC output voltage of 400 V and 650 V are shown in **Fig. 6**. Note that in order to account for the fact that the 6M-YR has twice the number of modules (rated for half the nominal power) compared to the 3M-YR and 3M-YR-U, the 6M-YR current stresses are increased by a factor of two in **Fig. 6**. As expected from (2), the 6M-YR module 1- Φ input current I_1 is elevated by approximately a factor of two compared to 3- Φ operation, and therefore the required filter component overdimensioning compared to 1- Φ operation of a standard 3M-YR (I_1 increased by a factor of three, cf. **Fig. 1b**) is reduced. In contrast, identical 3- Φ and 1- Φ module input current values I_1 result for the 3M-YR-U.

For the 6M-YR inductor I_L and semiconductor current I_{T1}, I_{T2}, I_{T3} the stress increase for 1- Φ operation is less pronounced compared to the module input current I_1 , as also the high-frequency current ripple impacts the resulting current RMS and peak values. Only power transistor T_4 faces a substantial current stress increase up to a factor of 2.5 given by the selected 1- Φ modulation strategy. However, the conduction

TABLE II: POWER STAGE DESIGN SPECIFICATIONS

	3M-YR / 3M-YR-U	6M-YR
f_s	100 kHz	100 kHz
Semi.	Cree C3M0021120K 1.2 kV, 21 m Ω (at $T_j = 25^\circ\text{C}$)	Cree C3M0040120K 1.2 kV, 40 m Ω (at $T_j = 25^\circ\text{C}$)
Unfolder	United SiC UF3SC120009K4S 1.2 kV, 8.6 m Ω (at $T_j = 25^\circ\text{C}$)	-
L	85 μH 2 x TDK EELP 43 (N97) 20 turns litz wire (71 μm)	170 μH 7x Magnetics E25/10 ($M\mu$ 60) 24 turns (1.5 mm enamelled wire)
C_a	3.5 μF 16 x Syfer X7R ^a , 0.47 μF , 1 kV	1.7 μF 8 x Syfer X7R ^a , 0.47 μF , 1 kV
C_{dc}	12 μF 48 x Ceralink 0.25 μF , 900 V	12 μF 48 x Ceralink 0.25 μF , 900 V

^aReferenced evenly to positive and negative DC-link rails.

stresses of T_4 (as well as the buck-boost inductor L) in each module could be further reduced in both 3- Φ and 1- Φ operation if during the clamping interval (i.e. T_1 and T_4 permanently on) also T_2 is turned on, such that a parallel conduction path to the negative DC-link rail is established.

As can be noted, the 3M-YR-U shows the most homogeneous component stress distribution in 1- Φ and 3- Φ operation and for the considered operating points. Hence **Fig. 6** clearly illustrates the tradeoff between modularity, 1- Φ buck-boost capability and component conduction stresses, where the 6M-YR (especially given the 1- Φ modulation strategy with reduced switching losses shown in **Fig. 3b.ii**) represents an interesting alternative topology.

B. Power Stage Performance Comparison

In the following a power stage efficiency and loss comparison among the considered topologies based on virtual prototypes is presented. The considered component realizations are listed in **Tab. II**, where 3M-YR and 3M-YR-U are realized (apart from the additional unfold bridge-leg for the 3M-YR-U) identically.

1200 V Silicon Carbide (SiC) semiconductors with Kelvin contact are employed in the buck and boost stages of all designs, and the selected 3M-YR (and 3M-YR-U) semiconductors (C3M0021120K) feature an on-state resistance of 21 m Ω . The semiconductor chip area for the 6M-YR is scaled to 50% to maintain the ratio of conduction and switching losses and accordingly the C3M0040120K (40 m Ω) is selected. The semiconductor switching losses are calculated by scaling the data presented in [11]. The unfold bridge-leg of the 3M-YR-U is realized with the lowest available on-state resistance of a commercial device, i.e. the UF3SC120009K4S with 8.6 m Ω . Given the fundamental-frequency operation of the unfold bridge-leg, its switching losses are neglected in the performance evaluation. The input capacitors are realized with ultra compact X7R ceramic capacitors, which are referenced evenly to the positive and negative DC-link rails to minimize the non-linear capacitance variation [12]. The specified capacitance value in **Tab. II** represents the resulting minimum capacitance value for the considered operating range, and the capacitor large-signal excitation losses are assessed based on [13]. The inductors of the 3M-YR are realized with litz wire and N97 ferrite cores, while for the 6M-YR iron powder cores

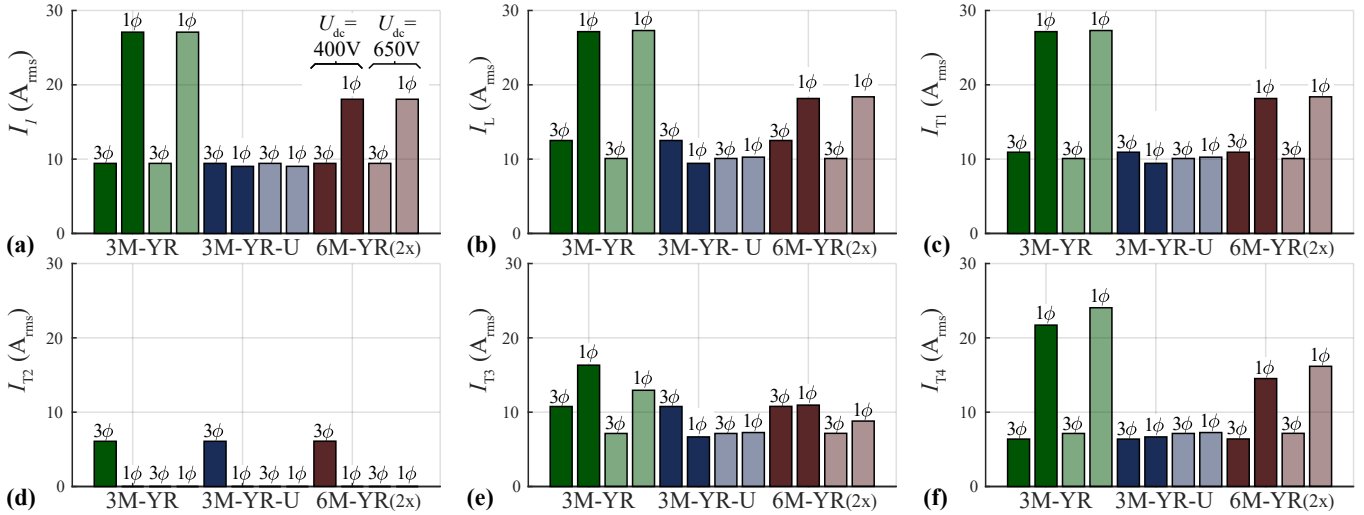


Fig. 6: Phase module component RMS current stresses of the 3M-YR (cf. **Fig. 1**), 3M-YR-U (with unfold bridge-leg, cf. **Fig. 2a**) and 6M-YR (cf. **Fig. 3a**) in 1- Φ (240 V_{rms} line-to-neutral voltage) and 3- Φ operation (400 V_{rms} line-to-line voltage) for two operating points with $P = 6.6$ kW and a DC output voltage of 400 V and 650 V. As the 6M-YR consists of six modules, its current stresses are scaled by a factor of two in order to allow a fair comparison. The component designators refer to **Fig. 2a** and **Fig. 3a**.

with high saturation flux density (without air gap) and solid wire is employed to allow a compact realization despite the larger component count. The conduction and core losses are calculated based on [14]. Last, to limit the high-frequency DC-link voltage variation 12 μ F of Ceralink ceramic capacitors are employed for all topologies, where the impact on the power stage loss performance is low and hence neglected. Note that for 1- Φ operation a power pulsation buffer is required to compensate for the inherent double-line frequency input power pulsation, where either a large electrolytic DC-link capacitor or an active power pulsation buffer can be employed [15] [16].

Fig. 7 presents the calculated efficiencies and loss distributions of the considered topologies ((**a**) 3M-YR, (**b**) 3M-YR-U and (**c**) 6M-YR) in 3- Φ ($U_{3\Phi} = 230$ V_{rms}) and 1- Φ ($U_{1\Phi} = 240$ V_{rms}) operation for a DC output voltage $U_{dc} = 400$ V over increasing output power and up to nominal power of 6.6 kW. The semiconductor switching losses are represented by hatched areas to allow differentiation of conduction and switching losses. In 3- Φ operation (cf. **Fig. 7a.i-c.i**), the designs show almost identical performance (losses of up to ≈ 100 W corresponding to an efficiency of $\approx 98.5\%$), which results due to the selected scaled realization of the 6M-YR modules (i.e. twice the inductance value and twice the semiconductor on-state resistance). Note that the 6M-YR inductor losses are elevated compared to the other topologies, which results due to the larger core-losses in powder core materials. However, the inductor realization with solid wire (instead of litz wire with more insulation material), as well as distributing the losses among six components (instead of three for the 3M-YR) allows improved heat dissipation, i.e. making the losses tolerable.

Then, in 1- Φ operation (cf. **Fig. 7a.ii-c.ii**), the loss and efficiency performance of the topologies differs massively. Note that $U_{dc} = 400$ V corresponds to pure boost operation in 1- Φ operation, such that for all topologies the buck stage A semiconductors cause only conduction losses. The 3M-YR

switching losses (cf. **Fig. 7a.ii**) reduce substantially compared to 3- Φ operation, as one of the three modules is not connected, while only one of the two active modules operates with PWM at a given point in time (the modulation presented in **Fig. 3b.ii** is employed). In contrast, the module currents elevated by a approximately a factor of three (compared to 3- Φ operation, cf. **Fig. 6**) cause the semiconductor conduction losses to increase faster with increasing output power. More critically, the considered 3M-YR design is constrained in 1- Φ operation by a power limit of ≈ 4 kW, which is imposed by the simulated inductor hot spot temperature exceeding 150 $^{\circ}$ C for higher output power levels. Then, the 3M-YR-U (cf. **Fig. 7b.ii**) shows substantially elevated switching losses (and hence worse part-load performance) compared to the 3M-YR, which results due to the permanent PWM operation of the three parallel modules (cf. **Fig. 2b.ii**). However, the semiconductor conduction and the inductor losses are even slightly lower compared to 3- Φ operation (the additional conduction losses of the unfold bridge-leg are up to 8 W, i.e. have marginal impact on the efficiency), such that again a nominal efficiency of 98.5% results. Last, the 6M-YR (cf. **Fig. 7c.ii**) shows reduced switching losses compared to 3- Φ operation, as only one of the two active module groups operates with PWM at a given point in time (cf. **Fig. 3b.ii**). The switching loss decrease is less accentuated than for the 3M-YR since all six modules are active, which in turn results in a lower conduction loss increase of the 6M-YR with power. However, the conduction stresses are still elevated compared to the 3M-YR-U and a reduced nominal efficiency of 98.0% results for the 6M-YR.

In summary, only the considered 3M-YR-U and 6M-YR power stage designs allow for 1- Φ and 3- Φ nominal power operation. Given the different circuit structures and modulation strategies, the 6M-YR shows improved 1- Φ part-load efficiency, while the 3M-YR-U virtual prototype achieves the maximum nominal power 1- Φ efficiency. With the 3M-YR-U only providing boost

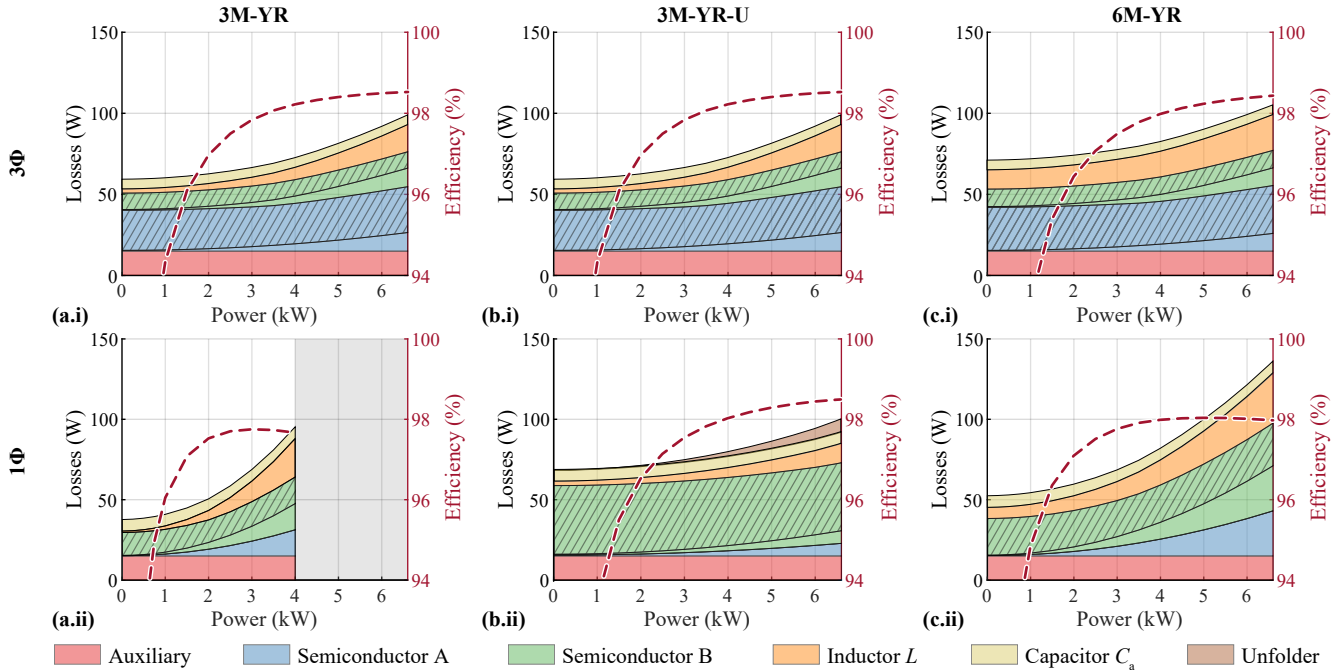


Fig. 7: Power stage efficiency and loss comparison of (a) 3M-YR, (b) 3M-YR-U and (c) 6M-YR in (x.i) 3- Φ ($U_{3\Phi} = 230 V_{\text{rms}}$) and (x.ii) 1- Φ ($U_{1\Phi} = 240 V_{\text{rms}}$) operation for a DC output voltage $U_{\text{dc}} = 400 V$ and output power up to 6.6 kW. The semiconductor switching losses are represented by hatched areas.

functionality in 1- Φ operation, the 6M-YR seems a very interesting topology candidate, and the corresponding EMI filter design process is discussed in the following.

V. EMI FILTER DESIGN

The relevant standard for on-board EV chargers [17] dictates high-frequency conducted grid emission limits which are based on the CISPR 11 residential class B limits [18] (cf. **Fig. 8**). The emission limits apply above 150 kHz and in the following a compliant EMI filter design is derived for the 6M-YR power stage specified in **Tab. II**.

As for the standard 3M-YR, the high-side buck stage semiconductor current i_{T1} (cf. **Fig. 3a**) is the most relevant quantity defining the EMI emissions and the required filter attenuation [19]. Note that i_{T1} in boost operation contains a switching-frequency triangular current ripple, while a switched, rectangular current i_{T1} results in buck operation. The maximum high-frequency RMS current ΔI_{HF} over one switching period of i_{T1} is approximately given by

$$\Delta I_{\text{HF}} = \begin{cases} \frac{1}{\sqrt{3}} \frac{1}{8} \frac{U_{\text{dc}}}{f_s L} \leq 3.2 A_{\text{rms}} & (\text{Boost}) \\ \hat{I}_1 \sqrt{1/d_{A,\text{min}} - 1} \leq 4.7 A_{\text{rms}} & (\text{Buck}). \end{cases} \quad (3)$$

In boost operation ΔI_{HF} depends on the inductance value L , as well as the switching frequency f_s . The maximum value $\Delta I_{\text{HF}} = 3.2 A_{\text{rms}}$ results for $U_{\text{dc}} = 750 V$ and a boost duty cycle $d_B = 0.5$ in both 1- Φ and 3- Φ operation. Then, assuming unity power factor (and neglecting the high-frequency inductor current ripple), ΔI_{HF} in buck operation is defined by the minimum buck duty cycle $d_{A,\text{min}}$ within one mains period and also depends on the peak module input current \hat{I}_1 . Note, that ΔI_{HF} does not depend on the power stage design parameters

f_s and L . Given the reduced buck effort in 1- Φ operation (cf. **Fig. 5a,b**), the maximum value $\Delta I_{\text{HF}} = 4.7 A_{\text{rms}}$ results in 3- Φ operation for $U_{\text{dc}} \approx 280 V$ (i.e. $d_{A,\text{min}} \approx 0.5$).

The high-frequency content of i_{T1} causes a corresponding input capacitor C_a voltage variation u_{C_a} (cf. **Fig. 3a**), which in case of the hypothetical absence of the EMI input filter is subject to the conducted emission limits. The high-frequency spectrum of the current i_{T1} and the input voltage u_{C_a} can be approximated by attributing ΔI_{HF} to a single switching-frequency component [20] and

$$\begin{aligned} \hat{I}_{T1}(nf_s) &= \frac{\Delta I_{\text{HF}}}{n^k} \\ \hat{U}_{C_a}(nf_s) &= \frac{\hat{I}_{T1}(nf_s)}{2\pi n f_s C_a} \end{aligned} \quad (4)$$

(n denominates the ordinal number). The current spectrum approximately decays with $k = 1$ in buck operation (switched current, -20 dB/dec) and $k = 2$ in boost operation (triangular current, -40 dB/dec) [20].

According to (3) and (4), the switching-frequency emission result to $\hat{U}_{C_a}(100 \text{ kHz}) = 133 \text{ dB}\mu\text{V}$ and with the worst case emissions resulting in buck operation, \hat{U}_{C_a} decays with -40 dB/dec (i.e. the current spectrum \hat{I}_{T1} and the impedance of C_a decay each with -20 dB/dec). The required EMI filter attenuation is then defined by the second switching frequency harmonic $\hat{U}_{C_a}(200 \text{ kHz}) = 121 \text{ dB}\mu\text{V}$. Considering an additional margin of 10 dB to the class B 200 kHz emission limit value of 63 dB μV , the required attenuation results to 67 dB which can be realized with two additional LC filter stages (cf. **Fig. 3a**).

The first filter stage comprises an inductance

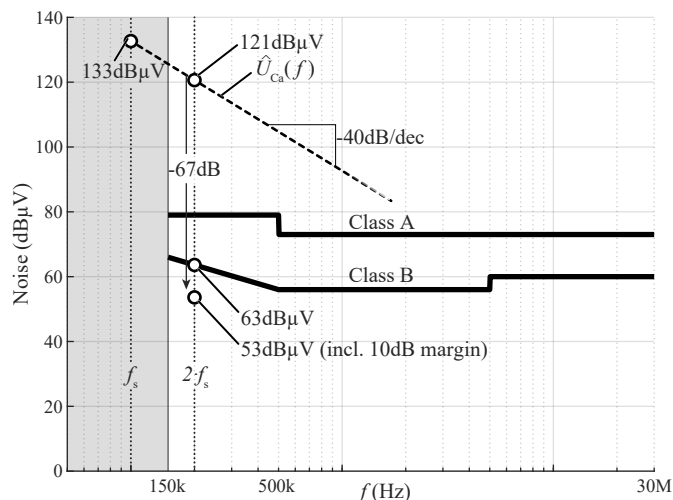


Fig. 8: CISPR 11 conducted EMI emission limits, estimated 6M-YR input capacitor voltage noise level \hat{U}_{Ca} and required EMI filter attenuation.

$L_{DM/CM} = 22\mu\text{H}$ (WE 74435582200) and again a DC-link referenced capacitor of $C_2 = 1.7\mu\text{F}$ (X7R, cf. **Tab. II**), hence providing attenuation to both differential and common mode noise. The second filter stage includes a six winding common mode choke $L_{CM} = 1.4\text{mH}$ (3x Vitroperm 500 40/25/15, 5 turns) and safety-rated capacitors $C_{CM} = 20\text{nF}$ to protective earth, such that also additional emissions resulting from the switch-node capacitances are attenuated [19]. Last, the leakage inductance of $L_{DM/CM}$ (typically in the range of 1%) forms a differential mode filter with $C_{DM} = 1.7\mu\text{F}$ (X7R, cf. **Tab. II**).

With the described filter structure, a CISPR 11 class B compliant 6M-YR system realization with a power density of up to $10\text{kW}/\text{dm}^3$ ($164\text{W}/\text{in}^3$, the EMI filter contributes approximately 30% of the converter volume) could be realized. The expected nominal efficiency results then to 98.1% in 3- Φ and 97.6% in 1- Φ operation.

VI. CONCLUSION

In this paper, 1- Φ operation at full (3- Φ) rated power of the 3- Φ Y-Rectifier is investigated, where three topologies are presented, namely the standard 3M-YR, the proposed 3M-YR-U with an additional unfold bridge-leg and extended CM EMI filter, as well as the novel 6M-YR, where the six converter modules are regrouped for 1- Φ and 3- Φ operation. The required modulation strategies of the 6M-YR are discussed and a cascaded PFC rectifier control concept is presented. Also, the main power component stresses of the presented topologies and virtual 6.6 kW, 3- Φ 400 V / 1- Φ 240 V, 200 V to 750 V DC prototype systems are compared. A (moderate) increase of the 6M-YR stresses for 1- Φ operation is found, such that a high converter performance can be realized, while buck-boost functionality is available both in 3- Φ and 1- Φ operation. Further, the EMI filter design process for the 6M-YR is discussed, and the results indicate the feasibility of a 6M-YR with power density of $10\text{kW}/\text{dm}^3$ ($164\text{W}/\text{in}^3$) and an expected nominal efficiency of 98.1% in 3- Φ and 97.6% in 1- Φ operation.

REFERENCES

- [1] IEC 62196, *Plugs, socket-outlets, vehicle connectors and vehicle inlets - conductive charging of electric vehicles*, Std., 2017.
- [2] SAE J1772, *SAE surface vehicle recommended practice J1772, SAE electric vehicle conductive charge coupler*, Std., 2009.
- [3] K. Stengert, "On-board 22 kW fast charger 'NLG6'," in *Proc. of the World Electric Vehicle Symposium and Exhibition (EVS27)*, Nov. 2013, pp. 1–11.
- [4] P. Ide, N. Froehleke, H. Grotstollen, W. Korb, and B. Margaritis, "Operation of a three-phase/three-level-rectifier in wide range and single-phase applications," in *Proc. of the IEEE Industrial Electronics Society (IECON)*, vol. 2, Nov. 1999, pp. 577–582 vol.2.
- [5] China Grid, "Electric vehicle charging equipment supplier qualification verification standard," 2017.
- [6] J. W. Kolar and T. Friedli, "The essence of three-phase PFC rectifier systems—part I," *IEEE Transactions on Power Electronics*, vol. 28, no. 1, pp. 176–198, Jan. 2013.
- [7] M. Antivachis, D. Bortis, L. Schrittwieser, and J. W. Kolar, "Three-phase buck-boost Y-inverter with wide DC input voltage range," in *Proc. of the IEEE Applied Power Electronics Conference and Exposition (APEC)*, Mar. 2018, pp. 1492–1499.
- [8] M. Antivachis, D. Bortis, D. Menzi, and J. W. Kolar, "Comparative evaluation of Y-inverter against three-phase two-stage buck-boost DC-AC converter systems," in *Proc. of the IEEE International Power Electronics Conference (IPEC - ECCE Asia)*, May 2018, pp. 181–189.
- [9] P. Papamanolis, F. Krismer, and J. W. Kolar, "22 kW EV battery charger allowing full power delivery in 3-phase as well as 1-phase operation," in *Proc. of the IEEE International Conference on Power Electronics (ECCE Asia)*, Aug. 2019, pp. 1–8.
- [10] K. Taniguchi, Y. Ogino, and H. Irie, "PWM technique for power MOSFET inverter," *IEEE Transactions on Power Electronics*, vol. 3, no. 3, pp. 328–334, Jul. 1988.
- [11] J. Azurza Anderson, G. Zulauf, J. W. Kolar, and G. Deboy, "New figure-of-merit combining semiconductor and multi-level converter properties," *IEEE Open Journal of Power Electronics*, vol. 1, pp. 322–338, Aug. 2020.
- [12] F. Maislinger, H. Ertl, G. Stojcic, C. Lagler, and F. Holzner, "Design of a 100 kHz wide bandgap inverter for motor applications with active damped sine wave filter," *The Journal of Engineering*, vol. 2019, no. 17, pp. 3766–3771, Apr. 2019.
- [13] D. Menzi, D. Bortis, G. Zulauf, M. Heller, and J. W. Kolar, "Novel iGSE-C loss modeling of X7R ceramic capacitors," *IEEE Transactions on Power Electronics*, vol. 35, no. 12, pp. 13 367–13 383, Dec. 2020.
- [14] P. Papamanolis, F. Krismer, and J. W. Kolar, "Minimum loss operation of high-frequency inductors," in *Proc. of the IEEE Applied Power Electronics Conference and Exposition (APEC)*, Mar. 2018.
- [15] H. Zhao, Y. Shen, W. Ying, S. S. Ghosh, M. R. Ahmed, and T. Long, "A single- and three-phase grid compatible converter for electric vehicle on-board chargers," *IEEE Transactions on Power Electronics*, vol. 35, no. 7, pp. 7545–7562, 2020.
- [16] Z. Liao and R. C. N. Pilawa-Podgurski, "Power harmonic elimination technique for using non-linear ceramic capacitors under large voltage swings for single-phase active power decoupling," in *Proc. of the IEEE Workshop on Control and Modeling for Power Electronics (COMPEL)*, Nov. 2020, pp. 1–7.
- [17] IEC 61851-21-1: *Electric vehicle conductive charging system - Part 21-1: Electric vehicle on-board charger EMC requirements for conductive connection to an AC/DC supply*, International Electrotechnical Commission (IEC) Std., 2017.
- [18] *C.I.S.P.R., Industrial, Scientific and Medical (ISM) Radio-Frequency Equipment - Electromagnetic Disturbance Characteristics - Limits and Methods of Measurement*, International Electrotechnical Commission (IEC) Std., 2015.
- [19] D. Menzi, D. Bortis, and J. W. Kolar, "EMI filter design for a three-phase buck-boost Y-inverter VSD with unshielded motor cables considering IEC 61800-3 conducted & radiated emission limits," unpublished (under review for the IEEE Transactions on Power Electronics).
- [20] K. Raggl, T. Nussbaumer, and J. W. Kolar, "Guideline for a simplified differential-mode EMI filter design," *IEEE Transactions on Industrial Electronics*, vol. 57, no. 3, pp. 1031–1040, Mar. 2010.